Journal of
MATERIALS RESEARCH

Silicon and zinc telluride nanoparticles synthesized by low energy density pulsed laser ablation into ambient gases

Douglas H. Lowndes and Christopher M. Rouleau
Solid State Division, Oak Ridge National Laboratory, P.O. Box 2008, Oak Ridge, Tennessee 37831-6056

T. G. Thundat
Life Sciences Division, Oak Ridge National Laboratory, P.O. Box 2008, Oak Ridge, Tennessee 37831-6123

G. Duscher
Solid State Division, Oak Ridge National Laboratory, P.O. Box 2008, Oak Ridge, Tennessee 37831-6056

E. A. Kenik
Metals and Ceramics Division, Oak Ridge National Laboratory, P.O. Box 2008, Oak Ridge, Tennessee 37831-6376

S. J. Pennycook
Solid State Division, Oak Ridge National Laboratory, P.O. Box 2008, Oak Ridge, Tennessee 37831-6056

(Received 17 December 1997; accepted 5 May 1998)

The size distributions of Si and ZnTe nanoparticles produced by low energy density ArF (193 nm) pulsed laser ablation into ambient gases were measured as a function of the gas pressure, P, and target-substrate separation, D_{ts}. For both Si and ZnTe, the largest nanoparticles were found closest to the ablation target, and the mean nanoparticle size *decreased* with increasing D_{ts}. For Si ablation into He, the mean nanoparticle diameter did not increase monotonically with gas pressure but reached a maximum near $P = 6$ Torr. High resolution Z-contrast transmission electron microscopy and energy loss spectroscopy revealed that ZnTe nanoparticles consist of a crystalline core surrounded by an amorphous ZnO shell; growth defects and surface steps are clearly visible in the crystalline core. A pronounced narrowing of the ZnTe nanocrystal size distribution with increasing D_{ts} also was found. The results demonstrate that the size of laser-ablated nanoparticles can be controlled by varying the molecular weight and pressure of an ambient gas and that nanometer-scale particles can be synthesized. Larger aggregates of both ZnTe and Si having a "flakelike" or "weblike" structure were formed at the higher ambient gas pressures; for ZnTe these appear to be open agglomerates of much smaller (~10 nm) particles.

I. INTRODUCTION

Recent pulsed laser deposition (PLD) experiments have demonstrated that by varying the pulsed laser wavelength, intensity, and ambient gas pressure, both the energy distribution and the nature of the ablated flux can be controlled.[1,3–12] Species ranging from highly energetic (⩾100 eV) atoms and ions up through clusters and nanocrystals can be produced, creating new opportunities for synthesis of novel thin-film materials and control of their properties.[1] Cluster and nanocrystal formation are greatly enhanced by ablating a material into a moderate-pressure (0.1–10 Torr) ambient gas.[2] With increasing gas pressure, the deposition flux changes from primarily atoms and ions to clusters and nanocrystals, the latter typically having diameters of 1 to 20 nm and containing from 10^2 to 10^6 atoms, with beneficial or detrimental consequences for film properties. For example, we recently grew *p*-type, nitrogen-doped epitaxial ZnTe films on GaAs(001) by ablating a ZnTe target into variable-pressure ambient N_2 gas.[3–5] However, the hole mobility exhibited a pronounced maximum in films grown at ~ 50 mTorr N_2 pressure, with lower mobilities for films grown at N_2 pressures ⩾ 100 mTorr. The decreased mobility was shown to be due to the onset of significant ZnTe cluster deposition with increasing N_2 pressure.[4,5]

Pure cluster-assembled or nanocrystalline films are of interest in their own right since they may have properties much different from films grown from a predominantly atomic/ionic flux, either because (i) of quantum confinement effects, (ii) the dominance of interfacial or defect electronic states (high surface/volume ratio), or (iii) because entirely new composite materials can be formed, for example by reaction with organic species present in the vapor phase.[6]

Thin-film deposits of nanocrystalline Si were produced recently by Yoshida *et al.*[7–9] by ablating a Si-wafer

 © 1999 Materials Research Society

target into He gas at a low pulsed ArF (193 nm) laser energy density, E_d, of 1 J/cm^2. Makimura *et al.*[10–12] also used a frequency-doubled Nd:YAG (532 nm) laser at much higher $E_d \sim 10$ J/cm^2 to deposit nanocrystalline Si films. Much smaller nanocrystals were obtained for ablation into He than into Ar.[13,14] Using a target-substrate separation, D_{ts}, of 7 mm, Yoshida *et al.* found that the mean size of the Si nanocrystals increased proportional to the 1/2.8 power of the He pressure, P, for $2 \leqslant P \leqslant 10$ Torr.[7] Using $D_{ts} = 19$ mm, Makimura *et al.* found qualitatively similar behavior, with the Si nanocrystal diameter varying as the 1/1.3 power of P for $0.5 \leqslant P \leqslant 20$ Torr.[10]

Because of interest in using PLD for both epitaxial and nanocrystalline semiconductor film growth and the importance of understanding cluster and nanoparticle formation, we have carried out systematic studies of the conditions required to form (or avoid forming) highly nanocrystalline semiconductor films. In this paper we report measurements of nanoparticle size distributions for both Si and ZnTe nanocrystals produced by pulsed ArF (193 nm) laser ablation into ambient He or N_2, respectively. The mean nanocrystal size was controlled by varying both the ambient gas pressure and the target-substrate separation. The first direct measurements of the internal structure of ZnTe nanocrystals also are reported here. For nano-Si, our experimental conditions were chosen to overlap, but extend to larger D_{ts}, the recent low-E_d experiments by Yoshida *et al.* that produced electroluminescent nano-Si films.[9] For nano-ZnTe, the experimental conditions overlap, but extend to much higher nitrogen pressures and shorter D_{ts}. The low-E_d ablation condition we earlier found was best for epitaxial growth of *p*-ZnTe:N.[3–5]

II. EXPERIMENTAL

Nanoparticles were deposited at room temperature onto Si(001) substrates (Wacker, both *p*- and *n*-type, 0.2–0.3 ohm-cm) in a load-locked UHV chamber. For each deposition, two Si strips (4 mm wide × 40 mm long) were positioned D_{ts} from the target. The two Si strips were mounted one above the other, facing the target, with a 5 mm gap between them through which the laser beam could pass. The Si substrates were dipped for 30 s in 5% HF to reduce the native oxide and hydrogen-passivate the surface, blown dry with N_2, and then were loaded immediately into the chamber.

A short-wavelength ArF (193 nm) laser was used at low energy density, E_d, in order to minimize ejection ("splashing") of large particulates from the targets. A 10 mm × 10 mm aperture was used to select the most uniform part of the laser beam, which was focused using two crossed cylindrical lenses. E_d was carefully calibrated using burn patterns on tempered, polished, and blued steel ribbon[15]; the focused beam area was ~5.4 mm^2. Insertion of 3 to 6 quartz plates and slight variations in the laser's pulse repetition rate were used to precisely reset the laser-pulse energy for each deposition. Targets were rotated at 20 rpm and the laser beam also was switched from one side of the target to the other after every 128 shots (making a ~12 mm diameter track) to further minimize target "coning" and production of large particulates. In connection with model calculations it should be noted that all targets were preablated to reach a steady state prior to nanoparticle deposition, typically by taking 2000 shots in vacuum while the substrates were held in the load lock. This produced a textured (nonspecular) target surface.

Silicon. Nanoparticles were deposited using 500 laser shots on Si(001) targets (Wacker, *p*-type, 0.2–0.3 ohm-cm) at a pulse energy of 56 mJ, corresponding to $E_d = 1.04\ (\pm 0.06)$ J/cm^2, in order to closely reproduce the laser conditions of Yoshida *et al.*[7–9] An ablation threshold $E_d{}^{th} \sim 0.76$ J/cm^2 was determined by observing the onset of visible Si plume formation in 1 Torr He. This $E_d{}^{th}$ value can be used to scale model calculations of nanoparticle formation to the deposition conditions used here. Nanoparticles were collected for static (no flow) He (99.9999% pure) pressures $P = 0.5$, 1.5, 4, and 10 Torr at target-substrate distances $D_{ts} =$ 10, 20, and 40 mm.

ZnTe. Nanoparticles were deposited using 500 laser shots on a fine-grained, hot-pressed ZnTe target (nominally 99.999% pure) at a pulse energy of 40 mJ, corresponding to $E_d = 0.74$ J/cm^2. This is close to the laser E_d used for our best *p*-ZnTe:N epitaxial films, grown in 50 mTorr of N_2.[3–5] ZnTe nanoparticles were collected at distances 4 cm $\leqslant D_{ts} <$ 12 cm from the target and at N_2 pressures of 0.15, 1.5, and 10 Torr. Molecular H_2 also was used in a few experiments.

Size distribution measurements. Images of the nanoparticles were obtained using a high-resolution (field emission) scanning electron microscope (HRSEM, Philips XL30/FEG) in secondary electron mode. The nominal probe size for the 20-kV condition used was ~2–3 nm, allowing detection, though not measurement, of nanoparticles with diameters approaching that limit. For conditions that produced large (10–20 nm) ZnTe nanoparticles, size distributions were determined by direct measurements of ~140 nanoparticles in the HRSEM images. The heights (~diameters) of nanoparticles too small for accurate HRSEM measurements (all Si and some ZnTe) were determined from tapping-mode atomic force microscope (TM-AFM, Nanoscope III, Digital Instruments, Santa Barbara, CA) images of 500 nm-square areas in two different regions of each specimen, corresponding to the center and left-of-center parts of the ablation plume. The TM-AFM has good vertical resolution ~0.05 nm, but its horizontal

resolution (apparent particle width) is limited by the finite size of the imaging tip. The apparent nanoparticle width is $W \sim 4(R_1R_2)^{1/2}$, where R_1 is the tip radius and R_2 is the nanoparticle radius. Thus, for measurements with a 10-nm tip, a 5-nm diameter nanoparticle can have an apparent width $W \sim 28$ nm. Consequently, the measured nanoparticle height was taken to be its diameter.

Nanoparticle size distributions (number density versus diameter) were obtained by statistical analysis of the TM-AFM images. Briefly, the images first were fit to a plane and flattened; then a statistical roughness analysis was carried out to determine the rms and average surface roughnesses. A grain size analysis was performed next by passing a series of planes through the nanoparticle images at various heights above the reference surface, using a height increment of one-half the rms roughness determined earlier. The number of nanoparticles terminating in each height interval then could be determined. This method of determining the nanoparticle size distribution tends to overestimate the number of very small nanoparticles because sufficiently jagged surfaces on larger particles may be counted as two (or more) particles. In contrast, direct visual analysis of plan-view HRSEM images inevitably *under*estimates the number of small particles, because particles below a certain size are ignored. Jaggedness also could result in an overestimate of the number of large particles, but that error can be avoided simply by viewing successive planar slices and noting where bifurcations occur. The nanoparticle height distribution also was viewed along particular line-scan directions on the surface as a rough check on each statistical analysis.

III. RESULTS

A. Silicon nanoparticle size distributions

AFM measurements of Si nanoparticle size distributions (nanoparticles/μm^2 versus mean diameter) are shown in Fig. 1. The measurements reveal that for He pressures in the range $1.5 \leqslant P \leqslant 10$ Torr, large nanoparticles are most numerous close to the target. With increasing target-substrate separation, the size distribution shifts toward smaller nanoparticles. In obtaining these distributions, occasional large, snowflake-like agglomerations that form increasingly at higher pressures (see Sec. V) were avoided, as were occasional μm-sized particulates ("splashing" from the target).

If each distribution is characterized by the average nanoparticle diameter, then the results shown in Fig. 2 are obtained. For all target-substrate separations in the range $10 \leqslant D_{ts} \leqslant 40$ mm, the mean Si nanoparticle size was maximized for $P \sim 6$ Torr under these ablation and deposition conditions. The existence of a maximum in the size distribution as a function of pressure is in striking contrast to the results of Yoshida *et al.*[7] and of Makimura *et al.*,[10] who found that the mean diameter of Si nanoparticles increased monotonically with the He pressure in this pressure range; their results also are shown in Fig. 2.

The absence of a normal (Gaussian) size distribution in the AFM measurements of Fig. 1, in contrast to HRSEM measurements of ZnTe nanocrystals (see below), apparently results from the ability of the AFM to detect quite small nanoparticles together with the need for an absolute cutoff (at approximately one standard deviation in surface roughness) in the minimum nanoparticle size that can be measured by the AFM nanoparticle counting method used here.

B. ZnTe nanoparticle size distributions, structure, and composition

Figure 3 and Table I show that by changing the N_2 or H_2 pressure or the target-substrate separation the average diameter of ZnTe nanoparticles could be varied over a wide range. Quite small ZnTe nanocrystals, with mean diameters of 1–2 nm, were formed either by ablating into N_2 at 150 mTorr or into H_2 at 1 Torr and collecting at $D_{ts} = 10$ cm (Table I).

The HRSEM data for $P[N_2] = 1.5$ Torr (Table I and Fig. 4) show that for fixed pressure the largest ZnTe nanocrystals were collected closest to the ablation target, just as was found for Si (Fig. 1). Figure 4 also reveals a pronounced narrowing of the ZnTe nanocrystal size distribution with increasing D_{ts} at fixed pressure. The HRSEM data for N_2 pressures of 1.5 and 10 Torr and fixed $D_{ts} = 4$ cm also reveal slightly smaller ZnTe nanocrystals at the higher pressure, perhaps indicating that the mean size of ZnTe nanocrystals reaches a maximum value at an intermediate N_2 pressure, similar to the behavior of Si shown in Fig. 2.

Table I also includes a comparison of the ZnTe nanocrystal diameters measured by HRSEM and AFM for $P[N_2] = 1.5$ Torr, $D_{ts} = 8$ cm, and shows that the

TABLE I. Mean diameters (and standard deviation) for ZnTe nanocrystals formed in N_2 or H_2 gas and collected at various target-substrate separations, D_{ts}, as measured by HRSEM or AFM.

Method	Gas	Pressure (Torr)	D_{ts} (cm)	Diameter (std. dev.) (nm)
HRSEM	N_2	1.5	4	31.4 (14.1)
			8	19.2 (7.9)
			12	15.8 (4.7)
	N_2	10	4	25.1 (7.4)
AFM	N_2	0.15	10	1.1
	N_2	1.5	8	9.4
	H_2	1	10	1.4
	H_2	10	5	4.8

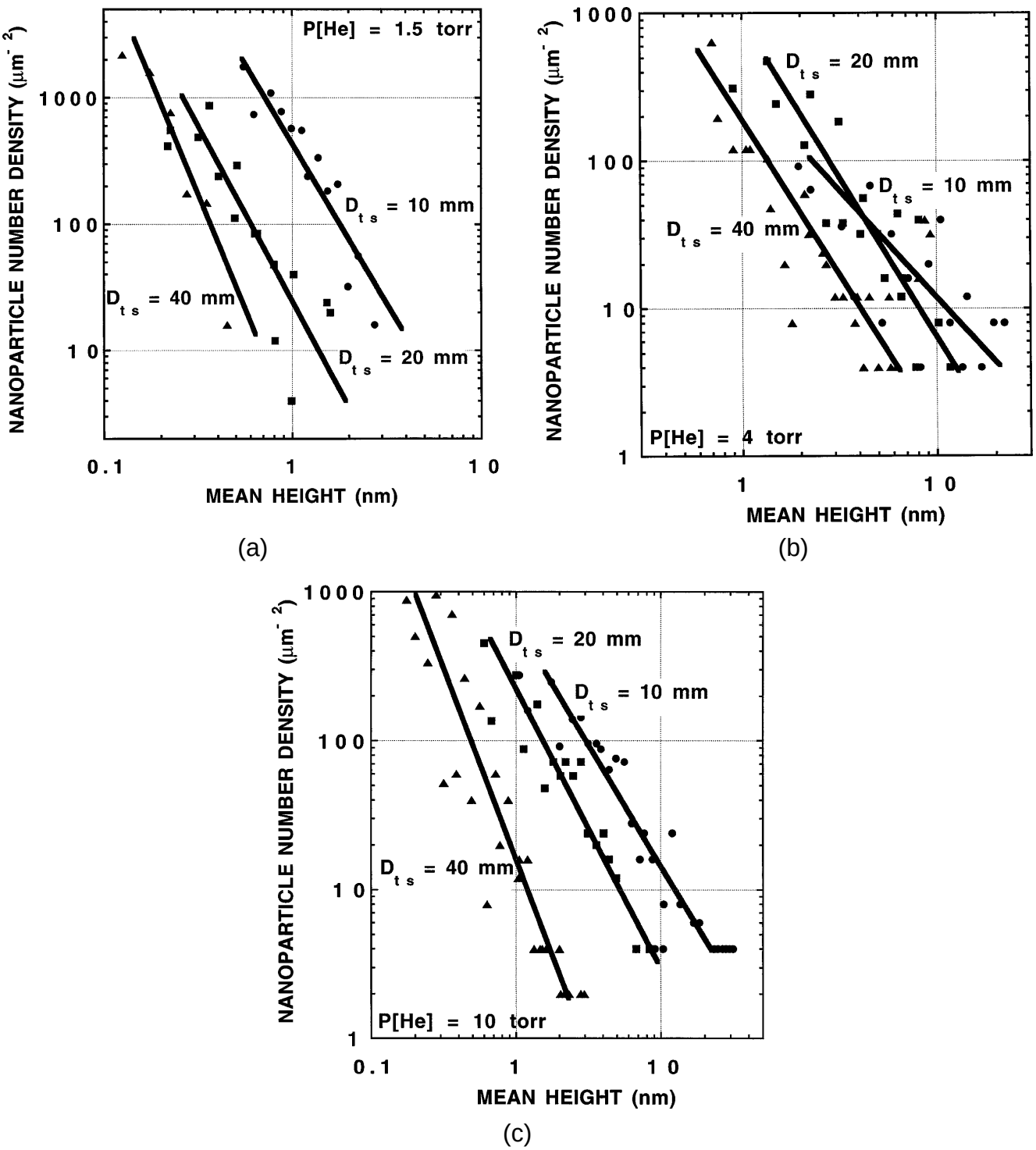

FIG. 1. Areal density of Si nanoparticles versus nanoparticle diameter at D_{ts} = 10, 20, and 40 mm for He pressures of (a) 1.5 Torr, (b) 4 Torr, and (c) 10 Torr, using 500 ArF laser pulses at 1.04 J/cm^2. This data was derived by analysis of AFM measurements, as described in the text.

mean diameter determined by AFM is about a factor of two smaller. This does *not* indicate any actual difference in the diameters measured by AFM and HRSEM for the same nanocrystal, but simply that the AFM data set includes many small nanocrystals that are missed in visual inspections of HRSEM images; consequently, the *mean* diameter determined by statistical analysis of AFM images is smaller.

HRZTEM was used to study in detail the microstructure, crystallinity, and composition of individual ZnTe

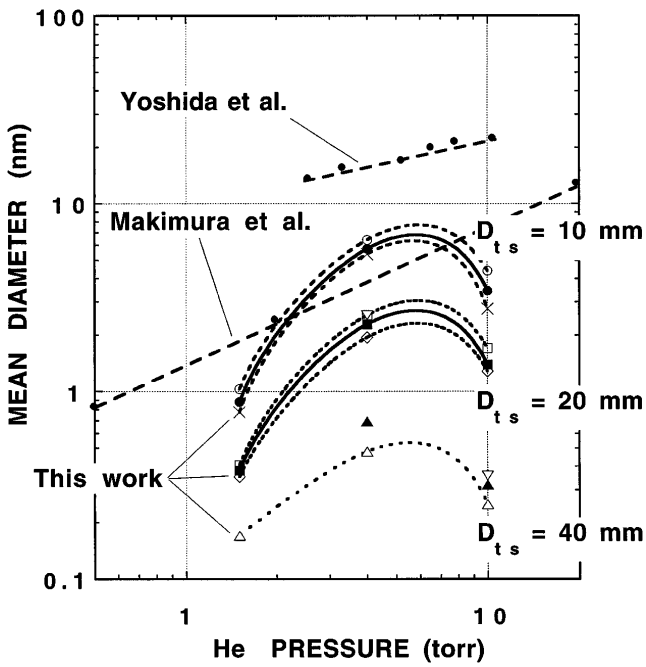

FIG. 2. Average Si nanoparticle diameter (height) versus He gas pressure during ablation, at target-substrate separations D_{ts} = 10, 20, and 40 mm. For each D_{ts} value, size distributions were measured at two locations on each substrate, corresponding to the center and left-of-center of the ablation plume (open symbols and dashed lines). The average of these measurements is shown by the solid symbols and line. Results from Refs. 7 and 10 also are shown.

nanoparticles in relation to their formation mechanism. The samples for these studies were briefly air-exposed but were loaded into the microscope within a few minutes after deposition. As shown in Fig. 5, atomic-resolution Z-contrast imaging revealed that both large (~10 nm) and small ZnTe (~2–3 nm) nanoparticles consist of a crystalline core surrounded by an amorphous ZnO shell [see Fig. 5(b)]. In fact, Z-contrast imaging detected what appear to be facets at the surface of the crystalline core as well as internal defect structures, including what may be a twin boundary and stacking faults within the larger nanocrystal in Fig. 5(a). Other AFM images, as well as HRSEM pictures, revealed that the largest ZnTe nanocrystals were formed by collisions in the N_2 gas that resulted in initial nanocrystallite growth followed by subsequent agglomeration with other nanocrystals.

Information about the structure and chemical composition of ZnTe nanocrystals was obtained by measuring electron energy loss spectra (EELS) point-by-point across the larger nanocrystal of Fig. 5 (top). The resulting high-resolution composition profile is shown in Fig. 5 (bottom). The O and Te EELS profiles and HRZTEM images reveal definitively that the nanocrystal has a crystalline ZnTe core surrounded by an oxidized, amorphous ZnO outer shell.

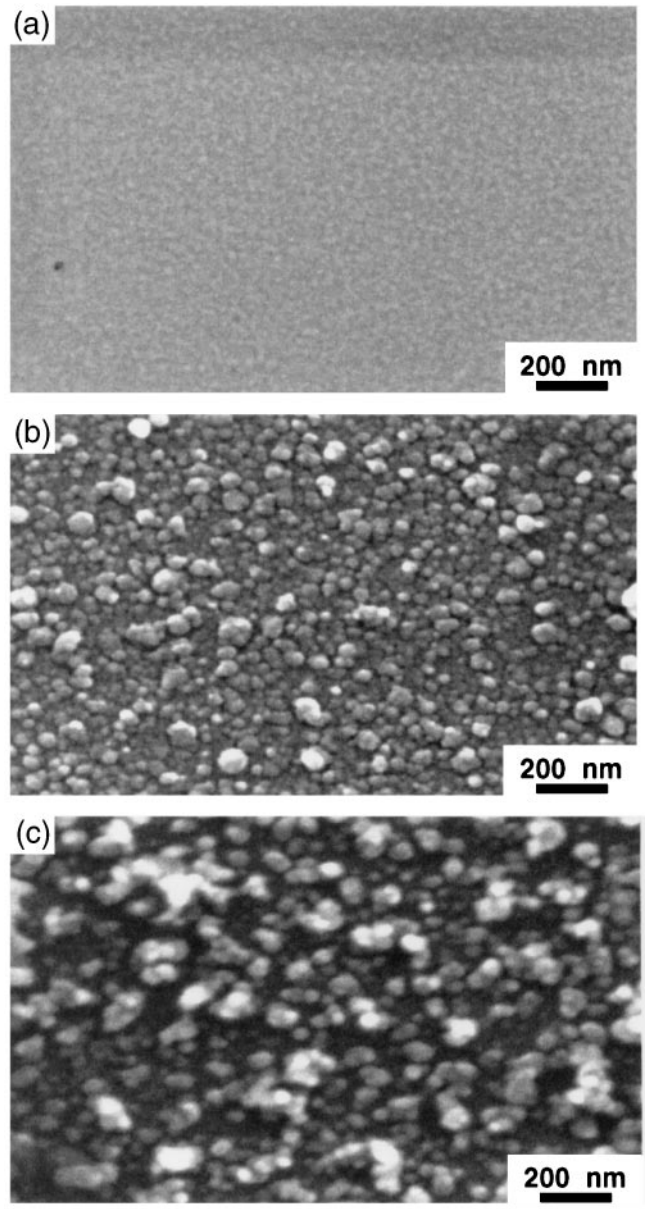

FIG. 3. HRSEM images of ZnTe nanocrystals deposited on a silicon substrate using 500 ArF laser pulses at E_d = 0.74 J/cm^2 in N_2 gas at (a) 150 mTorr, D_{ts} = 10 cm; (b) 1.5 Torr, D_{ts} = 8 cm; (c) 10 Torr, D_{ts} = 4 cm.

IV. OBSERVATIONS OF NANOPARTICLE FORMATION IN AMBIENT GASES

From time- and spatially-resolved ICCD-array measurements of light emission following Si ablation into He, Makimura *et al.*[10] developed a description of the propagation of ablated species that is consistent with earlier measurements by Geohegan *et al.*[16,17] of the interaction between ablated atoms/ions and ambient gases. Briefly, Makimura *et al.* reported that following Si target ablation the position of peak light emission moved with a constant velocity of 1.2×10^7 mm/s in vacuum, but evolved in

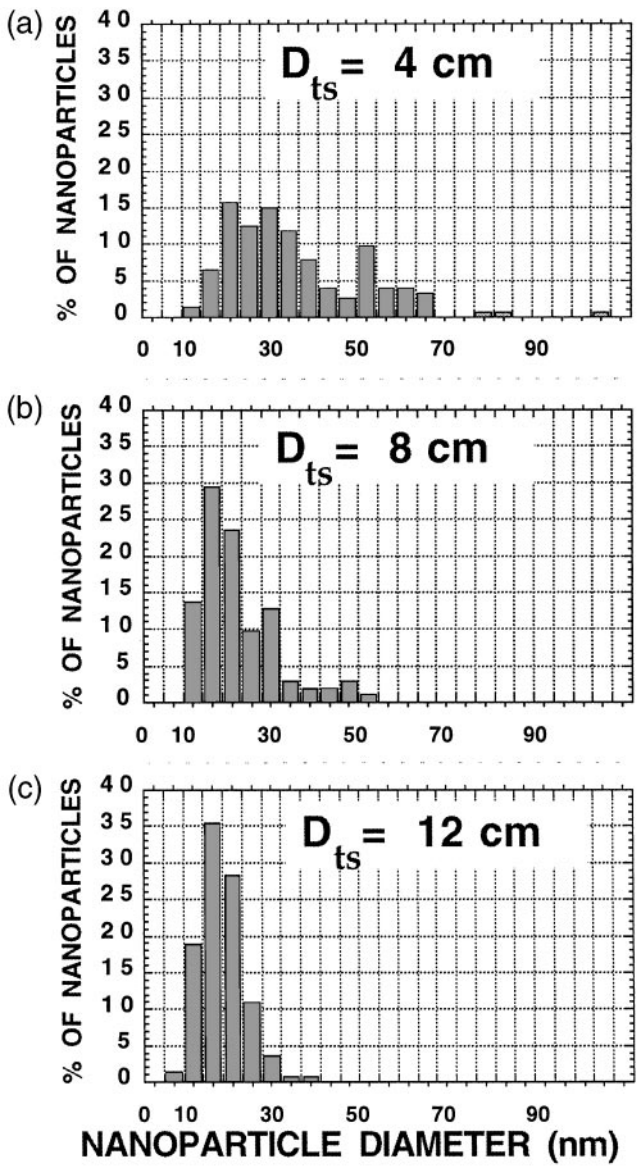

FIG. 4. ZnTe nanocrystal size distributions from HRSEM images for $E_d = 0.74$ J/cm^2, $P[N_2] = 1.5$ Torr and (a) $D_{ts} = 4$ cm; (b) $D_{ts} = 8$ cm; and (c) $D_{ts} = 12$ cm. Mean values and standard deviations for each distribution are included in Table I.

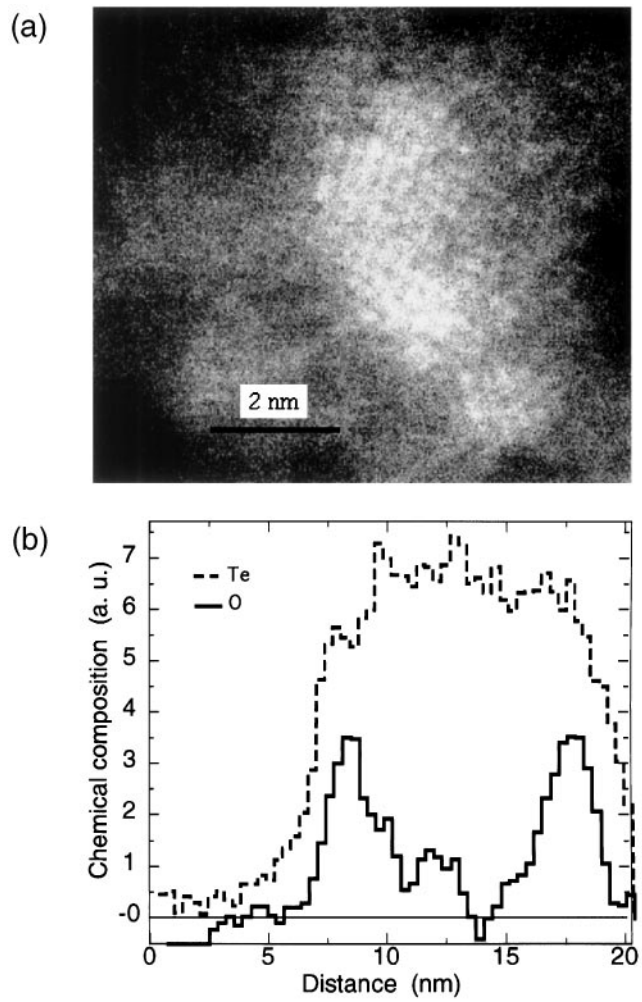

FIG. 5. (a) High-resolution Z-contrast TEM image of a large ZnTe nanocrystal (center) with a small nanocrystal attached (lower right). Crystalline lattice planes are clearly seen in the interiors of both nanoparticles. (b) Composition profile derived from spatially resolved EELS taken point-by-point across the larger ZnTe nanocrystal shown above (see text). The ZnTe nanocrystals were collected using $E_d = 0.74$ J/cm^2, $P[N_2] = 1.5$ Torr, and $D_{ts} = 8$ cm.

two stages when He gas was present. In 0.5 Torr of He, the peak emission position moved initially at an average velocity of 6×10^6 mm/s, but this was followed by a pronounced spatial spreading and slowing of the peak emission position until it became almost stationary at a distance of 12 mm from the Si target. In 2 Torr of He, the final (stationary) emission position was only 7 mm from the target. The second stage of motion is diffusive rather than ballistic.[10]

By correlating these measurements with AFM line-scan measurements of nanoparticle heights, Makimura *et al.* postulated a model for gas-phase Si nanocrystal formation.[10] Briefly, nanoparticles with nearly constant diameter were found on a substrate that was placed near or beyond the final position of light emission, but only smaller nanoparticles or no nanoparticles at all were found when the substrate was placed closer to the target. Furthermore, the Si nanocrystal size distribution did not depend on D_{ts}, if the substrate was placed farther from the target than the final position of light emission. Makimura *et al.* point out that gas-phase nanoparticle formation is strongly supported by the results that (a) the nanoparticle diameter increases with increasing He pressure and (b) nanoparticles are deposited on a substrate only when it is placed farther from the target than the final position of light emission. In this model, the first

stage of expansion is considered to be one of kinetic energy dissipation via collisions, while the second stage is one of particle agglomeration with the cohesive energy of nanocrystal formation dissipated into the gas.

The quantitatively different pressure dependences observed by Yoshida *et al.*[7] (using the 193 nm wavelength at $\sim$1 J/cm^2) and by Makimura *et al.*[10] (using the 532 nm Nd:YAG wavelength at $\sim$10 J/cm^2) were explained within this model by the formation in the latter experiments of Si atoms/ions in higher charge states and with much higher kinetic energy. These atoms/ions are expected to expand into a larger volume in the first stage, resulting in a lower atom density and the subsequent formation of smaller Si nanocrystals in the second stage.[10] Matsunawa *et al.* earlier observed exactly such a decrease in the mean size of metallic nanoparticles as the power density of a pulsed (msec) Nd:YAG laser was increased.[14] Matsunawa *et al.* also found that reducing the ambient Ar pressure resulted in much smaller metallic nanoparticles and a narrowing of their size distribution.[14]

Although time-resolved measurements and model calculations are necessary to fully understand the dynamics of nanocrystal formation, it was found in this work that direct visual observations of the spatial extent of luminescence in the ablation plume are strongly correlated with the dependences of nanoparticle size on ambient pressure and target-substrate separation. At a He pressure of 0.5 Torr, a bright orange plume extended slightly more than 20 mm out from the Si target and the same distance parallel to it. No significant deposits of Si nanocrystals were found for D_{ts} = 10 mm or 20 mm (average roughness $\sim$0.14 nm), i.e., no deposits within the luminescent plume, for P[He] = 0.5 Torr. Only a sparse distribution of large particulates was found at D_{ts} = 40 mm. However, for P[He] = 1.5 Torr, the luminescent orange plume was much shorter, extending only $\sim$7 mm out from the target and $\sim$10 mm parallel to it. As shown in Fig. 1(a), Si nanocrystals were the largest and most abundant at D_{ts} = 10 mm, just beyond the end of the luminescent plume. For P[He] = 4 Torr and 10 Torr, the luminescent plume dimensions perpendicular (parallel) to the target were $\sim$4 mm ($\sim$5 mm) and $\sim$2 mm ($\sim$2 mm), respectively. At these higher pressures, Si nanocrystals again were largest and most numerous closer to the target (D_{ts} = 10 and 20 mm) with primarily much smaller nanocrystals found at D_{ts} = 40 mm. These observations support the idea that nanocrystals are formed just outside (beyond) the highly excited (luminescent) part of the ablation plume when and where the kinetic energy of ablated species has been nearly completely dissipated by collisions.

When combined with the Si AFM data of Figs. 1 and 2, our plume observations reveal that, at any He pressure, the largest nanocrystals were deposited beyond but still close to the end of the luminescent plume, and the mean diameter of nanoparticles became systematically smaller with increasing D_{ts} (Figs. 1 and 2). The systematic decrease of nanoparticle diameter with increasing D_{ts} does not seem to have been present (or was simply not noticed) in earlier studies of laser-ablated Si nanocrystals. However, it is quite general in our data (occurring also for ZnTe nanocrystals, accompanied there by a narrowing of the size distribution, see Fig. 4 and Table I) and appears to be an important constraint on model calculations of nanoparticle formation.

V. FORMATION OF FRACTAL "SNOWFLAKE" OR "WEBLIKE" STRUCTURES AT HIGHER PRESSURES

Observations of the plume during ZnTe nanocrystal deposition in 1.5 Torr of N_2 revealed a purple luminescent region extending 4 to 5 cm out from the target, within which there was a blue core $\sim$3 cm long that occasionally touched substrates located at D_{ts} = 4 cm. In 10 Torr of N_2 the plume consisted of a bright blue core $\sim$1 cm long terminating in a blue ball at $\sim$2 cm, followed by a new region of pale yellow-orange luminescence that was not seen at $P[N_2]$ = 1.5 Torr and completely filling the space out to substrates placed at D_{ts} = 4 cm. HRSEM images such as those in Figs. 6 and 7 revealed that, in addition to nanocrystals, much larger aggregates having a "flakelike" or "weblike" structure were collected throughout the D_{ts} = 4–12 cm range under these conditions (static N_2 pressures of 1.5 and 10 Torr). Figure 6, for $P[N_2]$ = 1.5 Torr, shows that with increasing D_{ts} the areal density of flakes decreased but their size increased. The number of large flakes also increased with increasing N_2 pressure (compare the top panels in Figs. 6 and 7). Figure 8 shows that the flakes seen on the $\geqslant\mu$m scale actually are quite open agglomerations of much smaller ($\sim$10 nm-scale) particles. The flakelike agglomerations shown in Figs. 6–8 appear to be the source of the greatly increased yellow-orange luminescence during ZnTe ablation at $P[N_2]$ = 10 Torr.

A second, distinctly different, type of luminescence also was observed during Si nanoparticle deposition at He pressures of 4 and 10 Torr. A long "pencil" of weak orange luminescence extended back along the incident ArF excimer laser beam, apparently photoluminescence (PL) from larger particles or aggregates "floating" in the He gas and excited by the ArF laser beam. By quickly moving the substrate holder to produce turbulence this orange PL could be eliminated for a few laser shots but then was re-established, indicating that the larger aggregates could be swept out of the laser beam temporarily but then more were produced. At a static He pressure of 10 Torr the "pencil" of PL was well established along the ArF beam path and was present on every laser shot;

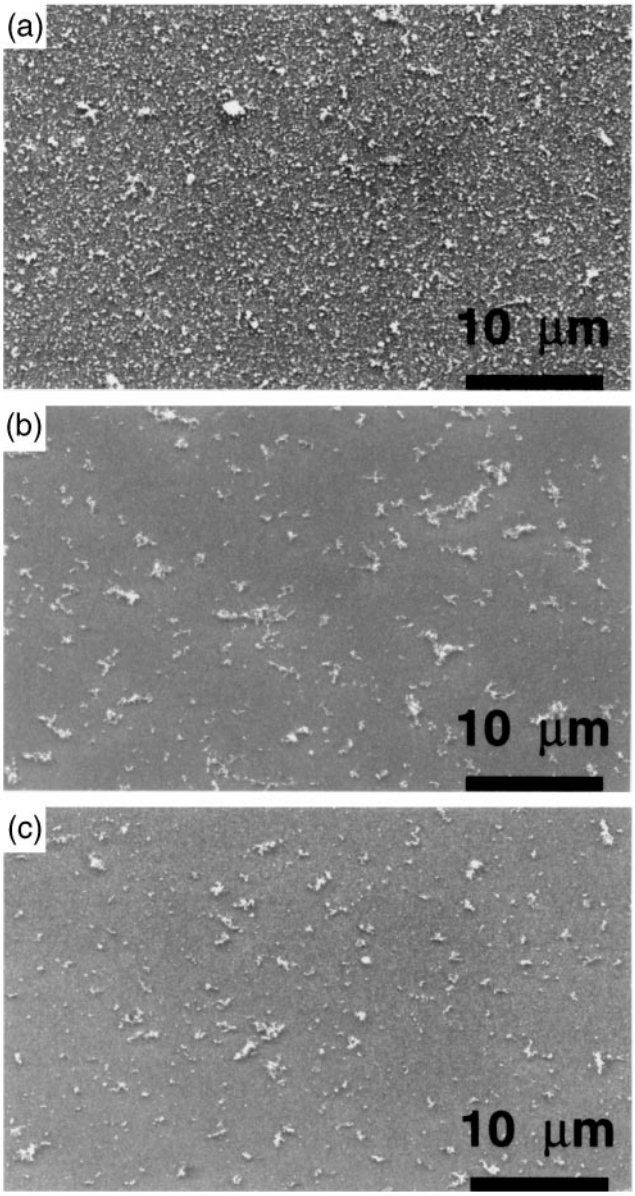

FIG. 6. ZnTe flakes deposited on Si substrates located at D_{ts} = (a) 4 cm, (b) 8 cm, and (c) 12 cm, after 500 ArF laser ablation pulses at $E_d = 0.74\ \mathrm{J/cm^2}$ into 1.5 Torr of static N_2.

this PL was strong out to ~13 mm from the target and weaker out to ~26 mm, indicating that the largest or most numerous aggregates were formed closer to the target. Indeed, inspection of the substrates on which Si nanoparticles were collected at 10 Torr He pressure revealed numerous larger Si aggregates (up to ~ 80 nm in diameter) at D_{ts} = 10 mm, but decreasing numbers as well as decreasing size of these aggregates at 20 and 40 mm. When the He flow rate through the chamber was increased to 72 sccm the "pencil" of PL fluctuated, suggesting that many of the larger aggregates were swept

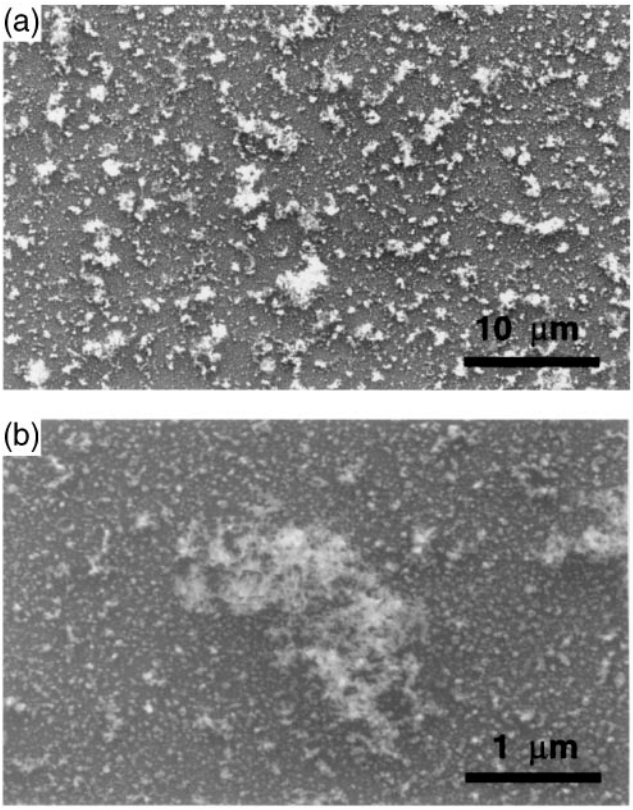

FIG. 7. (a) ZnTe "flakes" or "webs" collected on a Si substrate at D_{ts} = 4 cm after 500 ArF laser shots at $E_d = 0.74\ \mathrm{J/cm^2}$ into 10 Torr of static N_2. (b) High resolution image of one extended flakelike structure.

out of the ArF laser beam. At $P[\mathrm{He}] = 4$ Torr the pencil of PL was much less obvious though still clearly present.

Taken together, these observations demonstrate that larger aggregates of both ZnTe and Si were formed, grew mainly in the gas phase, and could be swept through the chamber by flowing gas.

VI. DISCUSSION

These experiments confirm the observation by Makimura *et al.* that there is negligible nanoparticle deposition if the collection substrate is placed within the fluorescent part of the ablation plume. In addition, three new results were obtained:

(1) In striking contrast to both Makimura *et al.*[10] and Yoshida *et al.*,[7] the mean diameter of Si nanoparticles did not increase monotonically with ambient gas pressure but instead reached a maximum near 6 Torr and then declined for higher pressures (Fig. 2).

(2) For both Si and ZnTe the *largest* nanoparticles were found closest to the ablation target (though always beginning beyond the fluorescent plume region) and the mean nanoparticle diameter *decreased* with increasing D_{ts}.

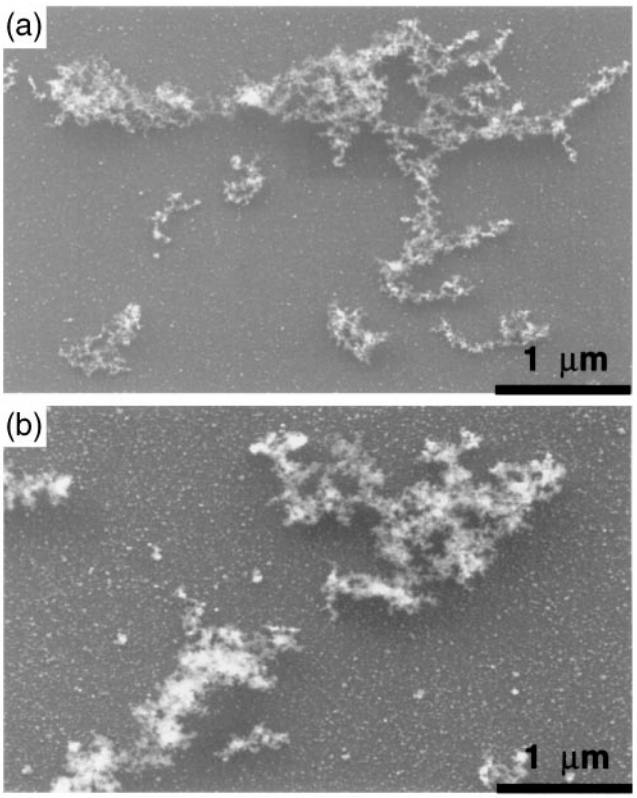

FIG. 8. High-resolution images of flakes collected at D_{ts} = (a) 8 cm and (b) 12 cm, following ZnTe ablation by 500 ArF laser pulses at $E_d = 0.74$ J/cm^2 into 1.5 Torr of static N_2.

(3) A pronounced *narrowing of the size distribution* with increasing D_{ts} (Fig. 4 and Table I) was found for ZnTe nanocrystals formed under these low-E_d ablation conditions.

A. Pressure-dependence of nanoparticle size

The maximum in the Si nanoparticle size distribution near P[He] ~ 6 Torr may be due to the relatively low laser E_d (193 nm) = 1.04 (±0.06) J/cm^2 as well as the different nanoparticle collection geometry that was used in this work. Makimura *et al.*[10] used a much higher E_d (532 nm) ~ 10 J/cm^2 to produce Si nanoparticles with mean diameters similar to those reported here (Fig. 2). In contrast, Yoshida *et al.*[7] reported using nominally the same E_d (193 nm) ~ 1 J/cm^2 to produce much larger Si nanoparticles (mean diameters increasing from >10 nm for P[He] = 2.5 Torr to ~20 nm at 10 Torr) at a D_{ts} of only 7 mm. The pronounced difference between our results and those of Yoshida *et al.* involves two factors:

(1) The E_d actually used by Yoshida *et al.* apparently was significantly higher than 1 J/cm^2. Their E_d was estimated from the laser pulse energy measured in front of the entry window and the laser burn area on Polaroid film.[13] The latter is susceptible to overestimating the laser spot size and therefore to underestimating E_d. There is clear evidence of a difference between the two sets of experiments since Yoshida *et al.* deposited a ~150-nm thick nano-Si film in about 30 min at 10 Hz,[13] while our deposition rate was much lower using E_d = 1.04 J/cm^2. Indeed, a recalculation indicates that Yoshida *et al.* used a laser E_d of ~1.8 J/cm^2 (or even higher) in their experiments.[13]

(2) Yoshida *et al.* mounted their Si substrates on a 4 cm × 4 cm square holder that was placed only 7 mm from the ablation target. This large holder undoubtedly strongly confined and reflected the ablation plume back into itself, greatly modifying its free expansion and drastically changing nanoparticle nucleation and growth conditions. In contrast, the relatively "open" collection geometry employed in this work, with two long Si-strip substrates placed both above and below a central ~5 mm gap through which the laser beam passed, may reduce reflection of the shock front that is formed when a target is ablated into a gas.[15] Consequently, both the time scales and the locations for nanoparticle growth would be expected to differ greatly in the two sets of experiments. The confinement and reflection of the plume in the experiments of Yoshida *et al.*, coupled with their much larger nanoparticle sizes, suggests that either the gas-phase growth conditions for their nanoparticles were much different or that much of their growth occurred after deposition on the substrate. *In situ*, time-resolved imaging measurements of the ablation plume are needed to fully understand these differences.

B. Dependence of nanoparticle size on D_{ts}

Yoshida *et al.* did not vary D_{ts},[13] while the model of Makimura *et al.* suggests that the nanoparticle size should increase with increasing D_{ts} if D_{ts} lies inside the "final" (stationary) position of plume luminescence, but should be approximately constant if D_{ts} lies outside. Matsunawa *et al.* reported an increase in the mean size of metallic nanoparticles formed by millisecond pulsed Nd:YAG laser ablation in 1 atm of Ar out to D_{ts} ~ 15 mm, with the metallic nanoparticles linking together but maintaining a similar size distribution at larger distances.[14] These results contrast with the systematic decrease in the size of both Si and ZnTe nanoparticles with increasing D_{ts} that was found in this work. This decrease seems to be a general characteristic of low-E_d ablation in the collection geometry used here but apparently was not noticed in the few previous ablation studies. For ZnTe nanocrystals the decrease in nanoparticle size was accompanied by significant narrowing of both the absolute and relative (% of mean value) size distributions. For example, for $P[N_2]$ = 1.5 Torr the mean size (and rms % deviation) of ZnTe nanocrystals decreased from

31 nm (±45%) at $D_{ts} = 4$ cm to 15.8 nm (±29%) at $D_{ts} = 12$ cm. As we now discuss, this narrowing may be quite useful if it can be developed further and exploited for quantum confinement.

C. Control of nanocrystal size and size distribution

These results demonstrate that the size scale for laser-ablated nanoparticles can be controlled through a combination of the molecular weight, *MW*, and pressure, *P*, of the ambient gas. For example, ZnTe nanocrystals formed in N_2 ($MW = 28$) and H_2 (MW = 2) at $P =$ 1 Torr and collected at $D_{ts} = 8$ cm had mean diameters (measured by AFM) of ~9 and ~1.4 nm, respectively. Decreasing the N_2 pressure to 0.15 Torr reduced the average nanocrystal diameter to ~1 nm, similar to that obtained by using higher H_2 at higher pressure. We note that Matsunawa *et al.* earlier found an absolute (but not relative) narrowing of the size distribution of laser-ablated metal and metal-alloy nanocrystals with decreasing gas pressure.[14]

Our data show that it should be possible to collect nanoparticles with a mean size of 3 (±1) nm (i.e., ±30%) by ablation into a low-*MW* gas at low pressure and large D_{ts}. Such nanocrystals are interesting mainly because at this length scale the quantum size effect substantially shifts the lowest quantized energy levels of electrons and holes and increases the energy of optical emission across the band gap.[18–20] Whether this can be exploited for light emission remains to be seen, since the size distributions of laser ablated nanoparticles still are relatively broad while the extent of oxidation, the need for surface passivation, and the relation of both to light emission are unclear. Nevertheless, nanocrystals of many elemental and compound semiconductors clearly can be synthesized by pulsed laser ablation, with the possibility of creating new nanocrystalline thin-film materials including layered and composite structures.[10]

We note that two methods for further reducing the spread of nanocrystal sizes also were reported recently:

(1) Camata *et al.* described a technique for size-classifying nanocrystals formed by any vapor-phase method.[21] A radial differential mobility analyzer was used to select nonagglomerated nanoparticles out of a polydisperse aerosol. The average nanocrystal size was selected simply by adjusting a voltage; size control to within ~15–20% was achieved in the 2–10 nm range.

(2) Ifuku *et al.* found that excess hydrogen radicals increase the density of nucleation but suppress the growth of Si nanocrystals formed in a high-frequency SiH_4 plasma cell.[22] By injecting a pulsed H_2 flow into a SiH_4 plasma cell they were able to control the relative amounts of time available for nucleation and for growth, thereby controlling both the nanocrystal size and size distribution. Si nanocrystals were deposited with a mean diameter of 8 nm and a narrow spread of only ±1 nm.

The principal limitation of both the Ifuku and Camata techniques appears to be fairly low surface coverage by size-selected nanoparticles ($\sim 10^{10}/cm^2$ to $10^{11}/cm^2$) after reasonable operating times.

D. Model calculations of nanocrystal formation

Wood and collaborators[23] recently tried to apply classical nucleation theory as outlined by Raizer[24] to describe nanoparticle formation in an ablation plume, first for a plume expanding into vacuum and then in an ambient gas. However, calculations using this model indicated that in laser ablation the initial expansion is so rapid that critical nuclei do not have enough time to form before the density falls to the "freezing" limit.[23] Moreover, if critical nuclei (with diameters of ~15 Å and containing ~40 atoms) could be formed in this way, then they should also form during ablation into vacuum and would be easily detectable by TEM or AFM. However, they do not seem to have been observed and the experiments described here confirm that the presence of an ambient gas is necessary for nanocrystal nucleation and growth. The model calculations of Wood *et al.* indicate that if critical nuclei had been present from the earliest stages of plume expansion into a gas then they would have grown to very large sizes, which also was not observed. Consequently, Wood *et al.* have postulated that the principal difference between a classical nucleation and growth scenario and the actual laser ablation situation is the *directed kinetic energy* of the plume constituents. It is only after this kinetic energy is mostly dissipated by collisions that stable dimers can form and grow into trimers, tetramers, etc., without being dissociated again.[23] This idea appears to be consistent with the data presented here though a full model remains to be developed.

E. Crystallinity of nanoparticles

For Si nanoparticles, Yoshida *et al.* obtained cross-sectional HRTEM images of ~3-nm and ~10-nm diameter spherical Si particles that revealed a core containing lattice planes with a spacing of 0.31 nm, nearly equal to the spacing of the (111) planes in crystalline Si. The core was surrounded by amorphous carbon from the microscope grid on which the nanoparticles were deposited.[7] Thus, at least the cores of the generally larger Si nanoparticles produced by Yoshida *et al.* were crystalline. As described above, we found a similar structure for ZnTe nanocrystals of various sizes. Whether the smaller Si nanoparticles produced in our work have a crystalline Si core surrounded by an oxide shell, as argued by Makimura *et al.*, is unknown.[10]

F. Future directions: Time-resolved *in situ* imaging

The results presented here provide useful constraints on model calculations of nanocrystal formation. However, the variations of mean nanoparticle size with ambient pressure and target-substrate separation also suggest that hydrodynamic flow or collisional phenomena may affect the nanocrystal size distribution, and perhaps can be exploited to collect nanoparticles with a narrower distribution. For example, how does placing a substrate in the ablation plume affect the flow and collisions of species in the plume? And how are nanoparticle nucleation and growth affected by collisions between incoming species and those reflected off a substrate? Such effects are not understood at this time and call for *in situ*, time-resolved imaging studies. *In situ* PL measurements can provide spatially and temporally resolved information about the connection between changes in plume hydrodynamics and the nucleation and growth of nanoparticles.[25] By such measurements it should be possible to determine (i) where in the ablation plume and on what time scale nanocrystals are formed; (ii) the effects of laser E_d, ambient gas pressure, and gas composition on the size and size distribution of nanocrystals; and (iii) hydrodynamic or collisional features of the plume expansion that yield especially favorable locations for nanocrystal collection.

At present we can only speculate whether the already-observed narrowing of the size distribution with increasing D_{ts} is related to such hydrodynamic or collisional features of the ablation plume. PL measurements are planned and should provide the experimental data needed to guide and test models for the formation of nanocrystals in ablation plume-ambient gas interactions.

VII. CONCLUSIONS

Several significant conclusions follow from this work. First, the mean size of nanoparticles produced by ablation into a gas and collected at some fixed distance does not necessarily increase monotonically with the gas pressure, as was found in earlier work.[7,10] Instead, for silicon ablated into helium the mean nanoparticle size reached a maximum at a pressure near 6 Torr, with smaller nanoparticles found at both higher and lower pressures, for each target-substrate separation studied. Data for ZnTe ablated into nitrogen show qualitatively the same behavior. Second, within the region in which nanoparticles can be found (beginning near the end of the luminescent plume and beyond), the largest nanoparticles are found close to the target and the mean nanoparticle size decreases at greater distances. Few nanoparticles were found very close to the target, i.e., within the luminescent plume. Third, HRZTEM measurements reveal that both large and small ZnTe (and presumably other compound semiconductor) nanoparticles have a crystalline ZnTe core. Fourth, a pronounced narrowing of the ZnTe nanocrystal size distribution with increasing D_{ts} was found. Fifth, differences in the average nanoparticle diameters determined by AFM and HRSEM result simply from the ability of the AFM to detect smaller particles; i.e., the AFM data set extends to smaller values. Sixth, the mean size of nanoparticles produced by ablation into a gas is a strong function of the molecular weight of the gas molecules (scattering cross section) and the gas pressure, with larger nanoparticles being produced by larger gas molecules or higher gas pressure. Finally, larger aggregates of both ZnTe and Si were formed at the higher ambient gas pressures. These aggregates grew mainly in the gas phase, produced luminescence in the ArF laser beam, and could be swept through the chamber by flowing gas. For ZnTe these aggregates have a "flakelike" or "weblike" structure and are loose, open agglomerates of much smaller (~10 nm) particles.

ACKNOWLEDGMENTS

The authors thank P. H. Fleming for assistance with analysis of the HRSEM nanoparticle images. This research was sponsored by the Oak Ridge National Laboratory, managed by Lockheed Martin Energy Research Corp. for the United States Department of Energy under contract DE-AC05-96OR22464.

REFERENCES

1. D. H. Lowndes, D. B. Geohegan, A. A. Puretzky, D. P. Norton, and C. M. Rouleau, Science **273**, 898 (1996).
2. D. E. Powers, S. G. Hansen, M. E. Geusic, A. C. Pulu, J. B. Hopkins, T. G. Dietz, M. A. Duncan, P. R. R. Langridge-Smith, and R. E. Smalley, J. Phys. Chem. **86**, 2556 (1982).
3. C. M. Rouleau, D. H. Lowndes, J. W. McCamy, J. D. Budai, D. B. Poker, D. B. Geohegan, A. A. Puretzky, and S. Zhu, Appl. Phys. Lett. **67**, 2545 (1995).
4. D. H. Lowndes, C. M. Rouleau, D. B. Geohegan, A. A. Puretzky, M. A. Strauss, A. J. Pedraza, J. W. Park, J. D. Budai, and D. B. Poker, in *Advanced Laser Processing of Materials—Fundamentals and Applications*, edited by R. Singh, D. Norton, L. Laude, J. Narayan, and J. Cheung (Mater. Res. Soc. Symp. Proc. **397**, Pittsburgh, PA, 1996), p. 107.
5. C. M. Rouleau, D. H. Lowndes, M. A. Strauss, S. Cao, A. J. Pedraza, D. B. Geohegan, A. A. Puretzky, and L. F. Allard, in *Advanced Laser Processing of Materials—Fundamentals and Applications*, edited by R. Singh, D. Norton, L. Laude, J. Narayan, and J. Cheung (Mater. Res. Soc. Symp. Proc. **397**, Pittsburgh, PA, 1996), p. 119.
6. W. M. K. P. Wijekoon, M. Y. M. Lyktey, P. N. Prasad, and J. F. Garvey, Appl. Phys. Lett. **67**, 1698 (1995).
7. T. Yoshida, S. Takeyama, Y. Yamada, and K. Mutoh, Appl. Phys. Lett. **68**, 1772 (1996).
8. Y. Yamada, T. Orii, I. Umezu, S. Takeyama, and T. Yoshida, Jpn. J. Appl. Phys. **35**, 1361 (1996).
9. T. Yoshida, Y. Yamada, and T. Orii, in *Technical Digest of the Inter. Electron Devices Mtg.*, San Francisco, CA, Dec. 8–11, 1996, IEEE, p. 417.

10. T. Makimura, Y. Kunii, and K. Murakami, Jpn. J. Appl. Phys. **35**, 4780 (1996).
11. T. Makimura, T. Sakuramoto, and K. Murakami, Jpn. J. Appl. Phys. **35**, L735 (1996).
12. T. Makimura, Y. Kunii, N. Ono, and K. Murakami, Jpn. J. Appl. Phys. **35**, L1703 (1996).
13. T. Yoshida, personal communication. In the deposition experiments the laser pulse energy was 60 mJ, measured before the quartz entrance window. Assuming a transmission factor of 0.91 and the 1×3 mm^2 area of Refs. 7 and 8, this corresponds to $E_d \sim 1.8$ J/cm^2.
14. A. Matsunawa, S. Katayama, A. Susuki, and T. Ariyasu, Trans. Jpn. Welding Res. Institute **15**, 233 (1986).
15. 0.003-inch $\times$ 3-inch #3 edge 1095 steel ribbon, tempered, polished, and blued; Amstek Metal, Joliet, IL.
16. D. B. Geohegan, Appl. Phys. Lett. **60**, 2732 (1992).
17. G. Duscher, D. B. Geohegan, A. A. Puretzky, and S. J. Pennycook, personal communication.
18. Al. L. Efros and A. L. Efros, Sov. Phys. Semicond. **16**, 772 (1982).
19. L. E. Brus, J. Chem. Phys. **79**, 5566 (1983).
20. L. Brus, J. Phys. Chem. **90**, 2555 (1986).
21. R. P. Camata, H. A. Atwater, K. J. Vahala, and R. C. Flagan, Appl. Phys. Lett. **68**, 3162 (1996).
22. T. Ifuku, M. Otobe, A. Itoh, and S. Oda, Jpn. J. Appl. Phys. **36**, 4031 (1997).
23. R. F. Wood, J. N. Leboeuf, K. R. Chen, D. B. Geohegan, and A. A. Puretzky, Fourth Int. Conf. on Laser Ablation (COLA'97), Monterey, CA, July 21–25, 1997; Surf. Sci. in press.
24. Yu. P. Raizer, Sov. Phys. JETP **37**, 1229 (1960).
25. D. B. Geohegan, personal communication and unpublished data.